Molecular Crystals and Liquid Crystals

Publication details, including instructions for authors and subscription information:
http://www.tandfonline.com/loi/gmcl20

Preparation and Properties of C_2-Symmetric Organic Radical Compounds Showing Ferroelectric Liquid Crystal Properties

Naohiko Ikuma [a], Yoshiaki Uchida [a], Rui Tamura [a], Katsuaki Suzuki [a], Jun Yamauchi [a], Yoshio Aoki [b] & Hiroyuki Nohira [b]

[a] Graduate School of Human and Environmental Studies, Kyoto University, Kyoto, Japan

[b] Graduate School of Science and Engineering, Saitama University, Saitama, Japan

Version of record first published: 05 Oct 2009

To cite this article: Naohiko Ikuma, Yoshiaki Uchida, Rui Tamura, Katsuaki Suzuki, Jun Yamauchi, Yoshio Aoki & Hiroyuki Nohira (2009): Preparation and Properties of C_2-Symmetric Organic Radical Compounds Showing Ferroelectric Liquid Crystal Properties, Molecular Crystals and Liquid Crystals, 509:1, 108/[850]-117/[859]

To link to this article: http://dx.doi.org/10.1080/15421400903065325

Mol. Cryst. Liq. Cryst., Vol. 509, pp. 108/[850]–117/[859], 2009

ISSN: 1542-1406 print/1563-5287 online
DOI: 10.1080/15421400903065325

Taylor & Francis
Taylor & Francis Group

Preparation and Properties of C_2-Symmetric Organic Radical Compounds Showing Ferroelectric Liquid Crystal Properties

Naohiko Ikuma[1], Yoshiaki Uchida[1], Rui Tamura[1], Katsuaki Suzuki[1], Jun Yamauchi[1], Yoshio Aoki[2], and Hiroyuki Nohira[2]

[1]Graduate School of Human and Environmental Studies, Kyoto University, Kyoto, Japan
[2]Graduate School of Science and Engineering, Saitama University, Saitama, Japan

We have synthesized a new class of liquid crystalline (LC) organic radical compounds **2***, which are the C_2-symmetric derivatives of the previously reported compounds* **1** *containing a chiral nitroxide unit and an ester group in the mesogen core, and their LC properties have been fully characterized. The enantiomerically enriched* **2** *showed N^* and SmC^* phases. Their LC phase transition behavior is similar to that of* **1***, whereas the ferroelectric properties of the SmC^* phase of (2S,5S)-***2*** differed from those of (2S,5S)-***1***. We discuss the origin of this difference in terms of their molecular structures optimized by molecular orbital calculations.*

Keywords: chiral nitroxide; chiral smectic C phase; ferroelectric liquid crystals; paramagnetic liquid crystals

INTRODUCTION

Endowing calamitic liquid crystals (LCs) with chirality results in the generation of chiral LC phases with helical superstructure, such as cholesteric (N^*) and chiral SmC (SmC^*) phases. Further addition of

The present work is supported by the Grant-in-Aid for Scientific Research (No. 19350067) from Japan Society for the Promotion of Science and the Asahi Glass Foundation (R.T.) and the Research Fellowships of the Japan Society for the Promotion of Science for Young Scientists (N.I. and Y.U.).

Address correspondence to Rui Tamura, Graduate School of Human and Environmental Studies, Kyoto University, Yoshida-nihonmatsu-cho, Sakyo-ku, Kyoto 606-8501, Japan. E-mail: tamura-r@mbox.kudpc.kyoto-u.ac.jp

paramagnetism to the chiral LCs is expected to provide novel advanced soft materials that can combine the optical and electrical properties of conventional chiral LCs with the magnetic properties of paramagnetic compounds [1–4]. For example, it is quite interesting to investigate whether magneto-electric effects are observable in the ferroelectric LC (FLC) state of paramagnetic materials. It is known that the magneto-electric effects originate from the interactions between magnetic-dipole and electric-dipole moments and are detectable as the influence of a magnetic (electric) field on the polarization (magnetization) of a material and *vice versa* [5].

In this context, we could obtain a series of prototypic all-organic chiral LC radical compounds **1** which have a nitroxyl group with a large electric dipole moment (3 Debye) as well as a polar ester group (1.8 Debye) used very often for the preparation of conventional FLCs (Fig. 1) [6]. Indeed, (2*S*,5*S*)-**1** ($n = 11 \sim 15$) showing an SmC^* phase exhibited ferroelectricity in a thin sandwich cell (4 μm thickness); the highest *P*s value of 24 nC cm^{-2} was recorded for (2*S*,5*S*)-**1** ($n = 13$) [7,8]. Furthermore, it has been found that both enantiomerically enriched and racemic samples of **1** exhibit unusual short-range intermolecular ferromagnetic-like interactions under weak magnetic fields in their LC phases [4,9,10].

To observe the magneto-electric effects, it would be essential to develop paramagnetic compounds showing a high *P*s value and magnetic interactions in the FLC state. Here we report the synthesis of enantiomerically enriched C_2-symmetric (2*S*,5*S*)-4-[5-(4-(4-alkoxyphenyl)

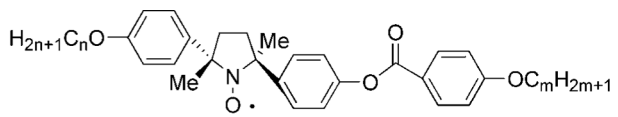

1

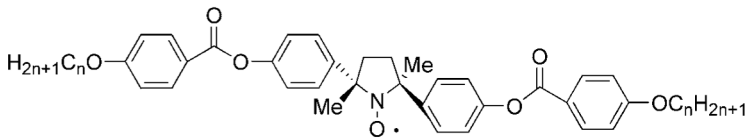

2a: n=8
2b: n=12
2c: n=13
2d: n=14
2e: n=15

FIGURE 1 Molecular structures of **1** and **2**.

calbonyloxyphenyl)-2,5-dimethylpyrrolidine-1-oxy-2-yl]phenyl 4-alkoxybenzoates (**2**), which have an additional polar ester group to improve the *P*s value compared to (2*S*,5*S*)-**1**, and discuss their ferroelectric properties (Fig. 1).

EXPERIMENTAL

General

Transition temperatures refer to the peak top of each transition curve by differential scanning calorimetry (DSC), which was performed at a scanning rate of 5°C/min. Enantiomeric excess (*ee*) was determined by HPLC analysis using chiral stationary phase column (Daicel Chiralcel OD-H, 0.46×25 cm), a mixture of hexane and 2-PrOH (9:1) as the mobile phase at a flow rate of 1.0 mL/min, and a UV-vis spectrometer (254 nm) as the detector. *P*s was measured by the triangular wave method at a frequency of 20 Hz in a 4 μm sandwich cell with ITO electrodes coated with polyimide in an electrical field of 10 V peak-to-peak. Tilt angles were measured by polarized optical microscopy (POM). Their g values and hyperfine coupling constants (a_N) were determined by electron paramagnetic resonance (EPR) spectroscopy in THF at 25°C. The variable temperature X-ray diffraction (XRD) patterns were recorded at a continuous scanning rate of 2° 2θ min^{-1} at a heating and cooling rate of 4°C min^{-1} using CuKα radiation (40 kV, 20 mA), with the intensity of the diffracted X-rays being collected at intervals of 0.02° 2θ.

General Synthetic Procedure of (2*S*,5*S*)-2 (Scheme 1)

Enantiomerically enriched nitrone (*R*)-**3** was prepared according to the published procedure [11]. The nitrone (*R*)-**3** (1.81 g, 16 mmol) was reacted with the Grignard reagent **4** (32 mmol) in THF (55 mL) at −78°C. The reaction temperature was slowly raised to room temperature. After being stirred overnight, the reaction mixture was poured into aqueous saturated NH_4Cl solution (100 mL), followed by extraction with CH_2Cl_2 and concentration in vacuo. The residue was dissolved in MeOH (30 mL) and oxidized by treatment with $Cu(OAc)_2$ (0.26 g), conc. NH_3 solution (2.1 mL), and O_2 bubbling until the solution color became dark blue. The solution was evapolated in vacuo, and the residue extracted by $CHCl_3$ (100 mL). The organic phase was washed with saturated aqueous $NaHCO_3$ solution (50 mL), dried over $MgSO_4$, and concentrated in vacuo to give the crude nitrone (*S*)-**5**. The crude (*S*)-**5** was reacted with **4** and the resulting crude

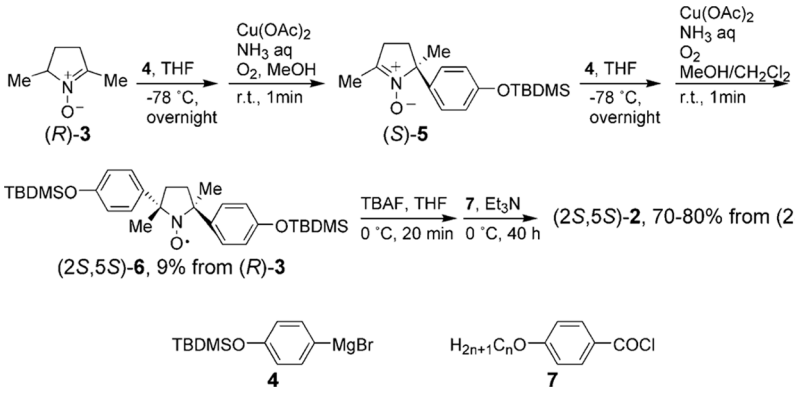

SCHEME 1 Synthesis of (2*S*,5*S*)-**2**.

addition product was oxidized by the same procedure. The crude nitroxide product was purified by column chromatography on silica gel (hexane/ether 99/1) to give pure (2*S*,5*S*)-**6** as yellow solid in 9% yield from (*R*)-**3**.

To (2*S*,5*S*)-**6** (0.4 mmol) in THF (10 mL) was added a THF solution of tetrabutylammonium fluoride (1 M solution, 1.0 mL) at 0°C. After being stirred at 0°C for 20 min, a solution of Et_3N (2.4 mL) and the *p*-alkoxybenzoyl chloride **7** (2.4 mmol) in THF (4 mL) was added. The reaction mixture was slowly warmed to 25°C and stirred for 40 h. Then the mixture was poured into aqueous $NaHCO_3$ solution and the aqueous mixture was extracted with ether (3×50 mL). The combined organic phase was dried over $MgSO_4$ and evaporated in vacuo. Column chromatography on silica gel (hexane/ether 9/1) of the residue gave pure (2*S*,5*S*)-**2** as yellow solid in 70–90% yield from (2*S*,5*S*)-**6**.

(2*S*,5*S*)-**2a** (93.5% *ee*): $[\alpha]_D^{26}$ −75.66 (c = 0.987, THF). EPR (THF): $g = 2.0059$, $a_N = 1.33$ mT. IR (KBr): ν 2928, 1735, 1603, 1507, 1448, 1369, 1248, 1206, 1166, 1076, 844, 762 cm^{-1}. Anal. Calcd for $C_{48}H_{60}NO_7$: C, 75.56; H, 7.93; N, 1.84; Found: C, 75.47; H, 7.98; N, 1.75.

(2*S*,5*S*)-**2b** (83.9% *ee*): $[\alpha]_D^{24}$ −62.77 (c = 0.971, THF). EPR (THF): $g = 2.0059$, $a_N = 1.33$ mT. IR (KBr): ν 2922, 1735, 1604, 1507, 1449, 1374, 1255, 1200, 1162, 1076, 846, 764 cm^{-1}. Anal. Calcd for $C_{56}H_{76}NO_7$: C, 76.85; H, 8.75; N, 1.60; Found: C, 76.69; H, 8.75; N, 1.58.

(2*S*,5*S*)-**2c** (90.6% *ee*): $[\alpha]_D^{24}$ −59.42 (c = 0.990, THF). EPR (THF): $g = 2.0059$, $a_N = 1.33$ mT. IR (KBr): ν 2912, 1735, 1603, 1507, 1374, 1250, 1199, 1160, 1052, 845, 766 cm^{-1}. Anal. Calcd for $C_{58}H_{80}NO_7$: C, 77.12; H, 8.93; N, 1.55; Found: C, 76.87; H, 8.89; N, 1.53.

(2*S*,5*S*)-**2d** (90.5% *ee*): $[\alpha]_D^{24}$ −56.85 (c = 0.986, THF). EPR (THF): $g = 2.0059$, $a_N = 1.32$ mT. IR (KBr): ν 2923, 1734, 1605, 1507, 1374, 1254, 1203, 1163, 1074, 846, 764 cm^{-1}. Anal. Calcd for $C_{60}H_{84}NO_7$: C, 77.38; H, 9.09; N, 1.50; Found: C, 77.08; H, 9.20; N, 1.49.

(2*S*,5*S*)-**2e** (88.0% *ee*): $[\alpha]_D^{24}$ −56.52 (c = 1.009, THF). EPR (THF): $g = 2.0059$, $a_N = 1.32$ mT. IR (KBr): ν 2915, 1734, 1603, 1507, 1369, 1248, 1201, 1161, 1050, 843, 762 cm^{-1}. Anal. Calcd for $C_{62}H_{88}NO_7$: C, 77.62; H, 9.25; N, 1.46; Found: C, 77.34; H, 9.13; N, 1.49.

RESULTS AND DISCUSSION

Characterization of LC Phases

The phase transition behaviour of (2*S*,5*S*)-**2** was characterized by DSC, POM, and XRD analysis, which were measured below 160°C because (2*S*,5*S*)-**2** instantly decompose in the isotropic phase above 160°C (Table 1, Figs. 2 and 3).

Similarly to the case of **1**, (2*S*,5*S*)-**2a** and (2*S*,5*S*)-**2b** with respective C8 and C12 chains exhibited only an N* phase, while (2*S*,5*S*)-**2c**–**2e** with longer alkyl chains showed N* and SmC* phases, with oily-streak and broken fan-shaped textures observed, respectively, on the cooling run (Table 1, and Figs. 2 and 3). Variable temperature XRD analysis verifies the existence of the N* and SmC* phases (Table 2 and Fig. 4).

To estimate the tilt angles of the SmC* phases, each molecular conformation with two structurally fixed linear anti-conformational alkyl chains was optimized by the PM3 semi-empirical calculation using PC Spartan'02 [12]. The optimized molecular geometries have a distorted zigzag structure that is advantageous for the appearance of an SmC* phase (Fig. 4b) [6,13]. The geometrical tilt angles were estimated to be close to 50° (Table 2).

TABLE 1 Phase Transition Temperature (°C) and ΔH (in parentheses, kJ/mol) of (2*S*,5*S*)-**2** on the First Heating Run

	Cr		SmC*		N*		I
(*S*,*S*)-**2a** (n = 8) (93.5% *ee*)	•	124.1 (36.7)			•	193.7 (1.5)	•
(*S*,*S*)-**2b** (n = 12) (83.9% *ee*)	•	101.7 (32.8)			•	165.3 (2.4)	•
(*S*,*S*)-**2c** (n = 13) (90.6% *ee*)	•	97.6 (38.2)	•	128.6 (1.1)	•	169.7 (3.5)	•
(*S*,*S*)-**2d** (n = 14) (90.5% *ee*)	•	99.0 (30.0)	•	141.3 (1.3)	•	169.8 (2.1)	•
(*S*,*S*)-**2e** (n = 15) (88.0% *ee*)	•	93.4 (35.7)	•	143.9 (2.1)	•	163.0 (1.2)	•

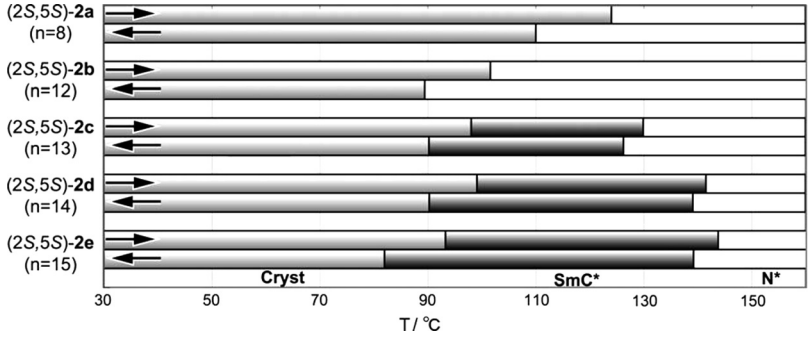

FIGURE 2 LC behavior of (2*S*,5*S*)-**2**.

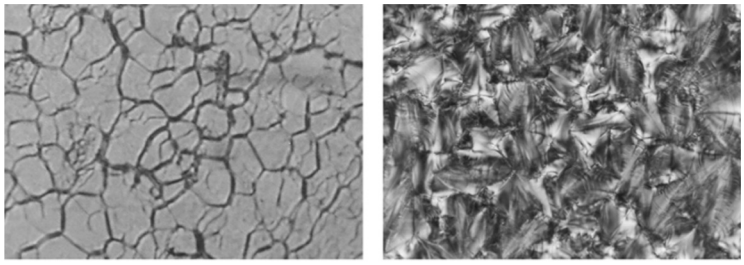

(a) (b)

FIGURE 3 Polarized optical micrographs of (2*S*,5*S*)-**2d** (90.5% *ee*). (a) oily-streaks texture at 150°C under homeotropic boundary conditions and (b) broken fan-shaped texture in a thin sandwich cell (4 μm) under homogenous planar boundary conditions at 130°C.

TABLE 2 Ferroelectric Properties Measured in the SmC* Phases of (2*S*,5*S*)-**2c-e**, Layer Distances, Calculated Molecular Lengths, and Geometrical Tilt Angles.

	$P_S(-10\ ^\circ)$ [nC · cm^{-2}][a,b]	$\theta\ (-10^\circ)$ [deg][b,c]	d [Å][d]	l [Å][e]	$\cos^{-1}(d/l)$ [deg][f]
(*S*,*S*)-**2c** (n = 13) (90.6% *ee*)	36 (116)[g]	42 (116)[g]	38.6 (115)[g]	57.5	48
(*S*,*S*)-**2d** (n = 14) (90.5% *ee*)	28 (129)[g]	43 (129)[g]	40.9 (130)[g]	59.8	47
(*S*,*S*)-**2e** (n = 15) (88.0% *ee*)	19 (129)[g]	44 (129)[g]	41.2 (110)[g]	62.3	49

[a]Spontaneous polarization. [b]Measured at a temperature 10°C below the phase transition from the N* phase to the SmC* phase during the cooling process. [c]Tilt angle measured by hot-stage POM. [d]Layer distance from XRD data. [e]Molecular length determined by a PM3 semiempirical calculation (PC Spartan'02). [f]Calculated geometrical title angle from d and l values. [g]Temperature (°C) in parentheses.

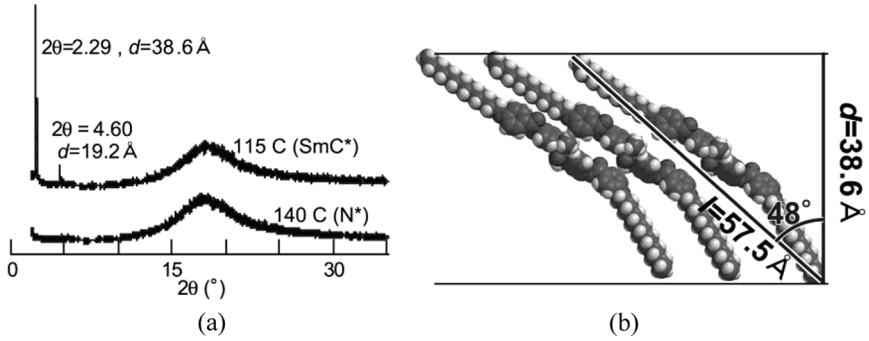

FIGURE 4 XRD patterns of (a) (2*S*,5*S*)-**2c** and (b) molecular structure of **2c** simulated by a PM3 geometry optimization.

Ferroelectric Properties

The magnitude of P_S and the optical tilt angles (θ) evaluated by oscilloscopic traces (Fig. 5a and b) and POM (Fig. 5c-f) of (2*S*,5*S*)-**2c**–**2e** are shown in Table 2 and Figure 6. On the cooling run from the N*-to-SmC* transition temperature, the P_S values rapidly increased (Fig. 6). The maximum $P_S(-10^\circ)$ value (36 nC cm^{-2}) observed for (2*S*,5*S*)-**2c** is larger than that (24 nC cm^{-2}) of (2*S*,5*S*)-**1** (n = 13) [7,8]. This increase in *P*s is consistent with the optimized molecular structure, in which two ester carbonyl groups direct to the same direction, resulting in the increase in the negative dielectric anisotropy. The experimental $\theta(-10^\circ)$ values of (2*S*,5*S*)-**2** were between 42° and 44°, which were smaller by $4 \sim 6^\circ$ than those estimated by the VT-XRD analysis and the PM3 calculation (Table 2). The tilt angles were so large that we could not measure the optical response times, because we observed only a bright-dark-bright or

FIGURE 5 Ferroelectric switching modes of (2*S*,5*S*)-**2** in a sandwich cell (4 mm) under homogeneous planar boundary conditions between crossed polarizers. (a) Polarization reversal current of (2*S*,5*S*)-**2d** measured by the triangular wave method at a frequency of 15 Hz in an electric field of 10 V peak-to-peak at 130°C. (b) Optical response of (2*S*,5*S*)-**2c** measured by the rectangular wave method at a frequency of 20 Hz in an electric field of 10 V peak-to-peak at 120°C: Transmitted light response (lower) and applied rectangular wave (upper). Applied DC voltage dependence of texture change of (2*S*,5*S*)-**2c** in the same area at 116°C: (c) +12 V, (d) 0 V, (e) −12 V, and (f) 0 V.

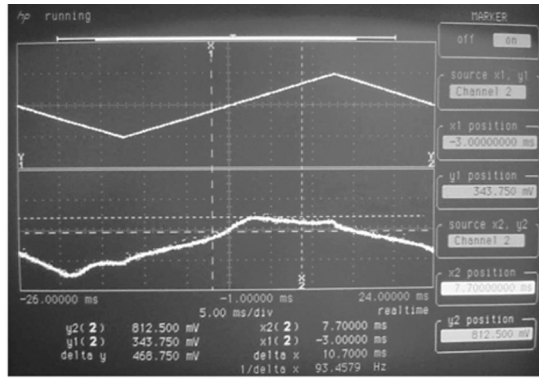

(a)

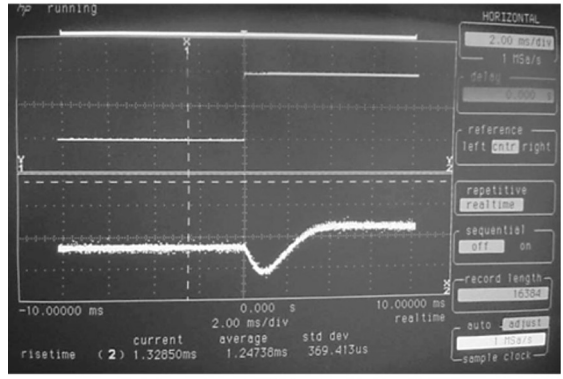

(b)

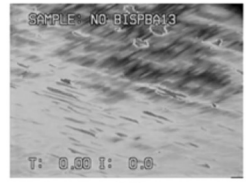

(c)

(d)

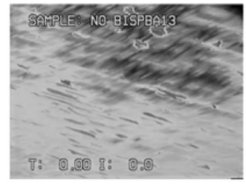

(e)

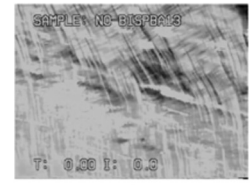

(f)

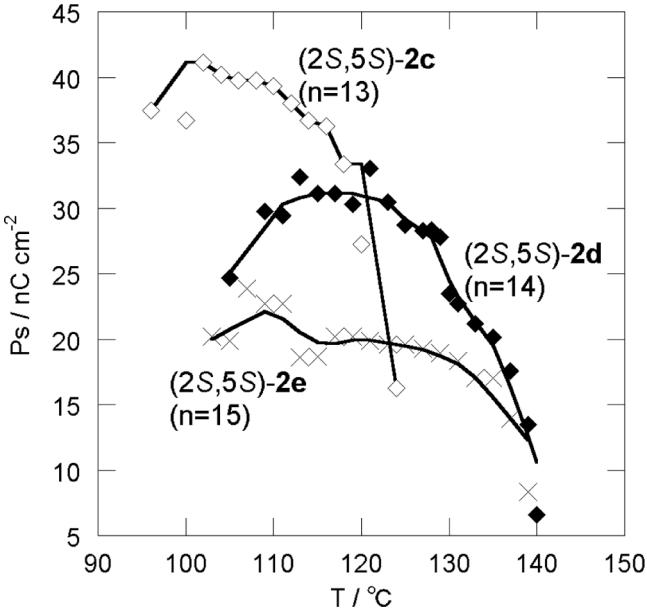

FIGURE 6 Temperature dependence of the *P*s values in the SmC* phases of (2*S*,5*S*)-**2c**–**e**.

dark-bright-dark texture change upon switching the polarity of the applied electric field (Fig. 5b).

Moreover, in contrast to the case of (2*S*,5*S*)-**1**, we observed the relaxation of the ferroelectric state of (2*S*,5*S*)-**2** in the same type of FLC cell, i.e., POM texture change by turning off the electric fields (Fig. 5c-f). At the same time, the textures in the two field-free states considerably differed from each other, suggesting the short-pitch SmC* nature and the incomplete formation of a helical superstructure in the FLC cell (Fig. 5d and f).

CONCLUSION

Thus, we could obtain a new class of chiral organic radical compounds showing FLC properties. One of them, (2*S*,5*S*)-**2c**, showed the highest *P*s value of 36 nC cm^{-2}, which was larger than that (24 nC cm^{-2}) of (2*S*,5*S*)-**1** (n = 13) [7,8]. Their unique C_2-symmetric molecular structure possessing one nitroxyl and two ester groups seems responsible for the resulting large tilt angles ($42 \sim 44^\circ$) in their SmC* phase. (2*S*,5*S*)-**2c** will be utilized as a soft magneto-electric material as well

as a real paramagnetic chiral LC probe or dopant to investigate the dynamic behavior of a given diamagnetic LC materials by EPR spectroscopy.

REFERENCES

[1] Griesar, K. & Haase, W. (1999). In: *Magnetic Properties of Organic Molecules*, Lahti P. M. (Ed.), Marcel Dekker: New York, p. 325.

[2] Serrano, J.-L. (1996). *Metallomesogens: Synthesis, Properties, and Applications*, VHC: Weinheim.

[3] Kaszynski, P. (1999). In: *Magnetic Properties of Organic Molecules*, Lahti P. M. (Ed.), Marcel Dekker: New York, p. 305.

[4] Likhtenshtein, G. I., Yamauchi, J., Nakatsuji, S., Smirnov, A. I., & Tamura, R. (2008). *Nitroxides: Applications in Chemistry, Biomedicine, and Materials Sciences*, VCH: Weinheim.

[5] Eerenstein, W., Mathur, N. D., & Scott, J. F. (2006). *Nature*, *442*, 759.

[6] Walba, D. M. (2003). *Top. Stereochem.*, *24*, 457.

[7] Ikuma, N., Tamura, R., Shimono, S., Uchida, Y., Masaki, K., Yamauchi, J., Aoki, Y., & Nohira, H. (2006). *Adv. Mater.*, *18*, 477.

[8] Ikuma, N., Tamura, R., Masaki, K., Uchida, Y., Shimono, S., Yamauchi, J., Aoki, Y., & Nohira, H. (2006). *Ferroelectrics*, *343*, 119–125.

[9] Uchida, Y., Ikuma, N., Tamura, R., Shimono, S., Noda, Y., Yamauchi, J., Aoki, Y., & Nohira, H. (2008). *J. Mater. Chem.*, *18*, 2950.

[10] Tamura, R., Uchida, Y., & Ikuma, N. (2008). *J. Mater. Chem.*, *18*, 2872.

[11] Einhorn, J., Einhorn, C., Ratajczak, F., Gautier-Luneau, I., & Pierre, J.-L. (1997). *J. Org. Chem.*, *62*, 9385

[12] Kong, J., White, C. A., Krylov, A. I., Sherrill, D., Adamson, R. D., Furlani, T. R., Lee, M. S., Lee, A. M., Gwaltney, S. R., Adams, T. R., Ochsenfeld, C., Gilbert, A. T. B., Kedziora, G. S., Rassolov, V. A., Maurice, D. R., Nair, N., Shao, Y., Besley, N. A., Maslen, P. E., Dombroski, J. P., Daschel, H., Zhang, W., Korambath, P. P., Baker, J., Byrd, E. F. C., Van Voorhis, T., Oumi, M., Hirata, S., Hsu, C.-P., Ishikawa, N., Florian, J., Warshel, A., Johnson, B. G., Gill, P. M. W., Head-Gordon, M., & Pople, J. A. (2000). *J. Comput. Chem.*, *21*, 1532.

[13] Walba, D. M., Slater, S. C., Thurmes, W. N., Clark, N. A., & Handschy, M. A. (1986). *J. Am. Chem. Soc.*, *108*, 5210.